Environmental Fluid Mechanics
https://doi.org/10.1007/s10652-024-09967-z

ORIGINAL PAPER

What does the volume-averaged water age distribution function reveal about flow fields in rectangular shallow reservoirs?

Benjamin Dewals[1] · Pierre Archambeau[1] · Sébastien Erpicum[1] · Michel Pirotton[1] · Eric Deleersnijder[2]

Received: 25 March 2022 / Accepted: 8 January 2024

Abstract
Shallow reservoirs are hydraulic structures widely used for water storage or as sedimentation tanks. Their design and sizing are intricate due to the complex flow fields developing in such structures, hence suitable indicators are needed to evaluate their hydraulic performance. Based on the outcomes of a depth-averaged computational model, we analysed the potential of the distribution function of the volume-averaged water age to unveil in a concise way valuable information on the flow field in rectangular shallow reservoirs. Ten different reservoir layouts were examined. In all cases, the shape of the computed distribution function reveals a remarkable amount of information on the flow field in the reservoirs. The distribution functions exhibit a sequence of steps, followed by an exponential decay, which may be related to fast and slow pathways travelled by water particles along their routes across the reservoirs. As such, the distribution function of the volume-averaged water age was found to provide valuable information for assessing the hydraulic performance of shallow reservoirs, while achieving an effective reduction in the problem dimensionality.

Keywords Hydraulic engineering, reservoir hydrodynamics · Shallow reservoir · Depth-averaged modelling · Water age distribution

1 Introduction

1.1 Context and objective

Shallow reservoirs are common hydraulic structures. They serve as storage or sedimentation tanks for stormwater management [1–5], and are part of green infrastructures such as constructed wetlands [6–9]. They are also used as settling basins in irrigation networks [10,

✉ Benjamin Dewals
b.dewals@uliege.be

[1] Research unit Urban & Environmental Engineering (UEE), Hydraulics in Environmental and Civil Engineering (HECE), University of Liege, Liege, Belgium

[2] Institute of Mechanics, Materials and Civil Engineering (IMMC) & Earth and Life Institute (ELI), Université Catholique de Louvain, Louvain-La-Neuve, Belgium

11] and for the treatment of waste water [12] or drinking water [13]. Shallow reservoirs serve as storage facility, in the form of service reservoirs in water supply systems [14], or as ancillary structures of hydropower schemes [15]. Among such reservoirs, many of them are rectangular in shape, or they may be closely approximated by a rectangle shape [10, 14, 16–18]. In geosciences, rectangular reservoirs have also been used as an idealization of non-engineered systems such as river mouths [19, 20].

The design, operation and maintenance of such reservoir poses multiple challenges. Sedimentation should be minimized in storage facilities, whereas the trapping efficiency is sought to be maximized in sedimentation tanks. For instance, the efficiency of sediment trapping in stormwater reservoirs has a considerable influence on the quality of water reaching the receiving body [6, 21]. Predicting the pattern of sediment deposits is of practical relevance for planning maintenance operations [12]. Similarly, water quality in drinking water reservoirs depends on water residence time and degree of mixing [14, 22].

All these processes are controlled by complex flow fields, involving large-scale turbulent structures, such as multiple recirculations [14, 23], which considerably influence short-circuiting and occurrence of low mixing regions. Hence, evaluating the hydraulic performance of shallow reservoirs may become an intricate task if it is directly based on the analysis of the flow field itself [6, 8, 18]. We suggest here that a valuable diagnostic tool for simplifying the assessment of flow fields in rectangular shallow reservoirs may be obtained by examining a particular type of timescale: the distribution function of the volume-averaged water age in the reservoir.

1.2 Background

Many experimental studies investigated flow fields in rectangular shallow reservoirs [1, 5, 24–28]. They revealed the occurrence of hydrodynamic instabilities, which make flow fields intricate to predict despite the simplicity of the structure geometry. Depending on the geometric and hydraulic conditions, distinct flow patterns develop in such reservoirs, as revealed by systematic laboratory observations [24–26, 28, 29]. For rectangular reservoirs with inlet and outlet channels located along their centreline, the flow pattern observed in steady state involves either a straight jet, or a reattached jet, or even a meandering jet [24–26, 28, 30]. Sediment trapping efficiency and mixing processes in reservoirs differ substantially from one type of flow pattern to another [1, 5, 31–33]. Therefore, in engineering applications, it is of utmost importance that the flow field be correctly predicted.

Computational models were successfully used to simulate velocity fields in shallow reservoirs, either in 2D [18, 34–39] or in 3D [1, 2, 5, 11, 17, 40, 41]. Most of these models include a sediment transport module [1, 2, 5, 11, 17, 33, 35]. The direct outcome of such computations are fields of primitive variables such as flow velocity, quantities characterizing flow turbulence, or depth of sediment deposits. These model outcomes constitute vast amounts of space-dependent data, which are not convenient to handle for effectively assessing the performance of reservoirs, e.g., in a design or optimization process. Indeed, as sketched in Fig. 1, the datasets involve at least two or three variables (velocity field) distributed in two to three dimensions depending on whether the hydrodynamics is described in 2D or in 3D. The large datasets generated by these computations need to be summarized into a reduced number of representative quantities to make performance assessment of reservoirs practicable.

Metrics such as the trapping efficiency achieve such simplification because they lump the whole complexity of flow and mixing processes into a single scalar quantity. Such a

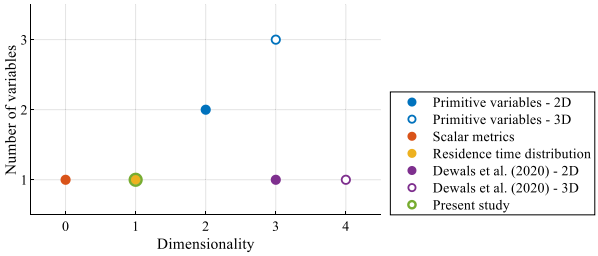

Fig. 1 Dimensionality and number of considered variables, as a function of the type of metric used for diagnosing the functioning of shallow reservoirs

metric achieves a remarkable dimension reduction (Fig. 1); but it misses a sizeable portion of the complexity of the processes. Trade-offs are needed between resorting to the whole set of primitive variables and adopting a single scalar quantity failing to reflect the diversity of the flow and constituent trajectories. Along this line, diagnostic methods based on time scales have been tested.

1.3 Time scales in shallow reservoirs

As emphasized by Lucas and Deleersnijder [42], timescales can provide a simplified, digestible (yet quantitative [43]) picture of the spatial complexity of many flow fields. The age of water particles is one such time scale. It is usually defined as the time elapsed since the water particle under consideration left a source region or entered the domain [44–47]. Water particles contained in a given region of the domain do not all have the same age since they are likely to have followed different routes to reach the considered region. Therefore, examining the distribution function of water age (i.e., the age histogram) is of particular relevance. The age of water particles exiting the domain at the reservoir outlet is called the transit time or the residence time. The distribution function of this quantity was used in several studies (Table 1).

Guzman et al. [6] determined residence time distributions (RTD) based on tracer studies in a laboratory facility. The RTD were used to compare the hydraulic performance of 54 reservoir layouts. The 10th percentile of the RTD, i.e. the time at which 10% of the injected mass exited the reservoir, was considered as a short-circuit indicator [48]. Similarly, Persson 8] computed the RTD for 13 reservoir layouts based on a 2D depth-averaged numerical model including an advection–diffusion equation for simulating the transport of a tracer. Positioning a subsurface berm or an island close to the reservoir the inlet was found to

Table 1 Studies analysing time scales in shallow reservoirs

Time scale	References	Statistical distribution	Spatial distribution	Volume-average
Residence time	Guzman et al. (2018); Persson et al. (1999; 2000); Moncho-steve et al. (2015); Xavier & Janzen (2017); Sonnenwald et al. (2018)	✓	–	–
Water age	Zhang et al. (2014)	–	✓	✓
	Dewals et al. (2020)	✓	✓	–
	Present study	✓	–	✓

reduce short-circuiting and increase the effective reservoir volume. Based on 3D computational fluid dynamics (CFD), Moncho-Esteve et al. [49], Xavier & Janzen [48] and Sonnenwald et al. [50] simulated the RTD at the outlet of reservoirs to analyse the effects of various design factors such as the inlet orientation and the presence of vegetation.

All these studies focused solely on the residence time, i.e., the effluent water age, in shallow reservoirs. In contrast, little attention was paid to the water age inside the reservoirs (Table 1), which is of importance to identify regions of water stagnation and grasp a deeper understanding of the reservoir functioning. Notable exceptions are studies by Zhang et al. [14] and Dewals et al. [51]. In the former, a commercial CFD model was applied to compute the spatial distribution of the mean water age (i.e., the mean time elapsed since entering the domain) in three service reservoirs of symmetric planform (rectangular, square and circular in shape). They found a similar residence time for the three reservoirs but distinct patterns of water ages, which hints at contrasts in the mixing mechanisms between the reservoir layouts. Nonetheless, only the mean water age was calculated by Zhang et al. [14] and not the whole distribution function of water age. Moreover, as the considered reservoirs are symmetric with respect to their centreline, Zhang et al. [14] simulated only one half of each reservoir, thereby assuming symmetry of the flow field. This conflicts with experimental observations, which have revealed large asymmetric recirculations in such shallow reservoirs [24, 26, 28, 35]. Therefore, the computations by Zhang et al. [14] do not properly capture the influence of the flow field on the spatial-dependence nor on the distribution function of water age in shallow reservoirs.

Unlike previous studies, Dewals et al. [51] computed the position-dependent water age distribution function in each computational cell (Table 1). It revealed that the distribution functions are multimodal and show complex features reflecting the multiple pathways followed by water particles in the reservoirs. This information is missed in analyses based on simple indicators such as the domain volume to discharge ratio or even the position-dependent mean water age. However, as shown in Fig. 1, the approach of Dewals et al. [51] reduces the number of variables of interest compared to the analysis of the primitive variables; but it fails to reduce the dimensionality. It even increases the dimensionality by one unit since the position-dependent age distribution functions computed by Dewals et al. [51] depend on the independent variables $\mathbf{x}$ and τ, where $\mathbf{x}$ is the position vector and τ the water age. The present study aims at assessing the value of examining the distribution function of the volume-averaged water age. This quantity enables a drastic reduction in the problem dimensionality compared to the approach of Dewals et al. [51] (Fig. 1), and it preserves more statistical information than in the calculations of Zhang et al. (2014) [14]. Our investigations are based on the same layouts of rectangular shallow reservoirs as considered by Dewals et al. [51], and they capitalize on the same computational results.

2 Data and methods

2.1 Geometric configurations and flow fields

Ten geometric configurations of experimental rectangular shallow reservoirs are studied here, with reservoir lengths L varying between 3 and 6 m, and reservoir widths B varying between 0.6 and 4 m (Fig. 2 and Table 2). The reservoirs are equipped with straight inlet and outlet channels of identical width b equal to 0.25 m. The reservoir expansion is defined as $\Delta B = (B - b)/2$. In all configurations, the bottom is horizontal in the reservoir as well

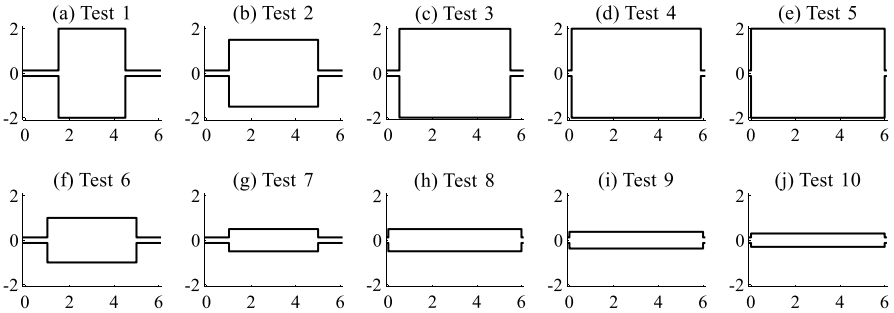

Fig. 2 Tested experimental configurations of shallow reservoirs. Distances are in meters

Table 2 Geometric characteristics of tested reservoir configurations, with characteristic time scales $T_m = V/Q$ and $T_j = L/U$, where V is the reservoir volume, Q the volumetric flow rate, L the reservoir length and U the average flow velocity in the inlet channel

Test ID	L (m)	B (m)	L/B (-)	$\Delta B/b$	T_m (s)	T_j (s)
Test 1	3	4	0.75	7.5	343	21
Test 2	4	3	1.33	5.5	343	29
Test 3	5	4	1.25	7.5	571	36
Test 4	5.8	4	1.45	7.5	663	42
Test 5	6	4	1.50	7.5	686	43
Test 6	4	2	2.00	3.5	229	29
Test 7	4	1	4.00	1.5	114	29
Test 8	6	1	6.00	1.5	171	43
Test 9	6	0.75	8.00	1	129	43
Test 10	6	0.6	10.00	0.7	103	43

as in the inlet and outlet channels. In all tests, the flow rate was kept constant and equal to $Q = 0.007$ m^{3}s^{-1}, while the downstream flow depth was set to $h = 0.2$ m. These geometric and hydraulic settings correspond to laboratory experiments conducted at EPFL Lausanne [52].

For the ten rectangular shallow reservoirs shown in Fig. 2, Camnasio et al. [52] computed the flow fields using a shallow-water model coupled with a depth-averaged $k-\varepsilon$ turbulence model [53]. The computations were performed based on a finite volume scheme and a Cartesian grid with a spacing of 0.025 m. The model provides the spatial distribution of flow depth, depth-averaged velocity, as well as depth-averaged turbulent kinetic energy and dissipation rate. The flow fields are displayed in Figure S1 in Supplement, while the computed flow depth h is virtually constant all over the reservoir.

In the tested configurations, three types of flow patterns may be distinguished:

- for relatively short reservoirs ($L/B < 1.5$, Tests 1–4), a straight, detached jet crosses the reservoir from the inlet to the outlet, with one flow recirculation on each side, both of them extending over the whole length of the reservoir;
- for reservoirs of intermediate length ($1.5 \leq L/B < 5$, Tests 5–7), the jet reattaches on one of the sidewalls, with a small recirculation on the same side as the reattachment point and, on the opposite side, a larger recirculation extending over the whole reservoir length;

- for relatively long reservoirs ($5 \leq L/B$, Tests 8–s10), the jet reattaches on one of the sidewalls, with a small recirculation on the same side as the reattachment point and, on the opposite side, a larger recirculation extending only over a portion of the reservoir length (i.e., a second reattachment point is present on the side opposite to that of the first one).

Only in the case of relatively short reservoirs ($L/B < 1.5$) the flow pattern is symmetric with respect to the reservoir centreline, while it is asymmetric in all other cases.

For each reservoir configuration, two time scales may be easily evaluated:

- $T_m = V/Q$ is defined as the ratio of the reservoir volume V to the flow rate Q (subscript m stands for "mixed");
- $T_j = L/U$ is defined as the ratio of the reservoir length L to the average flow velocity U in the inlet channel (subscript j stands for "jet").

Each characteristic time corresponds to the residence time of a hypothetical configuration, as sketched in Fig. 3. The former (T_m) refers to a perfectly mixed reservoir (Fig. 3a), and the latter (T_j) to a reservoir in which the inlet jet would undergo no diffusion, and continue as a plug flow over the whole reservoir length, with a width identical to that of the inlet channel (Fig. 3b). In general, T_m is considerably larger than T_j. Here, the ratio of T_m to T_j depends only on the reservoir aspect ratio $\Delta B/b$, since $T_m/T_j = 1 + 2\ \Delta B/b$. Hence, this ratio is unable to reflect the influence of the reservoir length on flow processes.

2.2 Water age distribution

The flow and turbulence fields computed by Camnasio et al.[52] were used by Dewals et al. [51] to determine the statistical distribution of water age throughout the reservoirs under steady conditions. The space- and age-dependent distribution function $c(x,y,\tau)$ was computed, where x and y denote the horizontal spatial coordinates and τ the age (as an independent variable). The physical dimension of the age distribution function $c(x,y,\tau)$ is the inverse of a time, and it is defined as follows: in an elementary volume $h(x,y)\ \delta x\ \delta y$, the volume of water whose age ranges between τ and $\tau + \delta\tau$ tends towards $c(x,y,\tau)\ h(x,y)\ \delta x\ \delta y\ \delta\tau$ when δx, δy and $\delta\tau$ tend towards zero. Notation $h(x,y)$ refers to the flow depth in the reservoir. The age distribution function satisfies the following constraint [51]:

$$C(x,y) = \int_0^\infty c(x,y,\tau)\, d\tau = 1 \tag{1}$$

with $C(x,y)$ the "water concentration", which, obviously, is identically equal to unity.

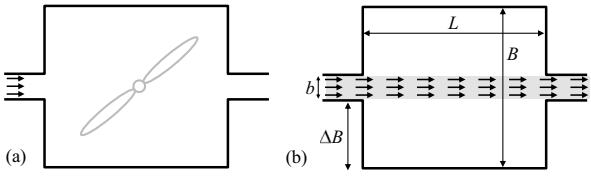

Fig. 3 **a** Sketch of a perfectly mixed reservoir. **b** Sketch of a reservoir crossed by a jet undergoing no diffusion. The grey shaded area corresponds to a plug flow region

Here, we additionally evaluate the spatially-averaged, steady, age distribution function $\mu(\tau)$, i.e. the volume average of $c(x,y,\tau)$ over the whole reservoir:

$$\mu(\tau) = \frac{1}{V}\int_{\Omega} h(x,y)\; c(x,y,\tau)\; d\Omega \tag{2}$$

with Ω the planar extent of the reservoir. Function $\mu(\tau)$ may be interpreted as follows: the volume of water whose age ranges between τ and $\tau + \delta\tau$ tends towards $\mu(\tau)\, V\, \delta\tau$ when $\delta\tau$ tends towards zero, i.e. $\mu(\tau)\, \delta\tau$ is the fraction of the volume reservoir whose age belongs to the interval $[\tau, \tau + \delta\tau]$. Function $\mu(\tau)$ satisfies the following identity:

$$\int_0^{\infty} \mu(\tau)\, d\tau = 1 \tag{3}$$

as can be easily demonstrated by combining Eqs. (1) and (2).

The distribution function $\mu(\tau)$ takes a particular value for $\tau = 0$, irrespective of the reservoir configuration [45]. Indeed, since water entering the reservoir is assumed to have an age equal to zero, the volume of water whose age is in the interval $[0, \delta\tau]$ tends towards $Q\,\delta\tau$ when $\delta\tau \to 0$. This same volume is also given by $V\,\mu(0)\,\delta\tau$ for $\delta\tau \to 0$. It comes:

$$Q\,\delta\tau = V\mu(0)\delta\tau \qquad \Rightarrow \qquad \mu(0) = \frac{Q}{V} = \frac{1}{T_m} \tag{4}$$

A closed form expression for function $\mu(\tau)$ can be derived for two hypothetical cases:

For a perfectly mixed reservoir of volume V and crossed by a constant flow rate Q (as sketched in Fig. 3a), the local age distribution function is independent of the position in the reservoir, so that $\mu(\tau)$ is simply equal to $c(\tau)$:

$$\mu(\tau) = c(\tau) = \frac{1}{T_m} e^{-\frac{\tau}{T_m}} \tag{5}$$

Note that, for this solution, $\mu(0) = 1/T_m$, in accordance with Eq. (4).

In the case of a plug flow (e.g., in the jet region if the inlet jet undergoes no diffusion over the whole length of the reservoir, as sketched in Fig. 3b), the local age distribution function writes:

$$c(x,\tau) = \delta\left(\tau - \frac{x}{U}\right) H\left(T_j - \tau\right) \tag{6}$$

with δ and H representing the Dirac delta function and the Heaviside step function, respectively. Consequently, the age distribution function spatially-averaged over the plug flow region reads:

$$\mu(\tau) = \frac{1}{T_j} H\left(T_j - \tau\right) \tag{7}$$

3 Numerical results

Based on the spatially-distributed water age distribution function $c(x,y,\tau)$ computed by Dewals et al. [51], we evaluated here the volume-averaged age distribution function $\mu(\tau)$ using Eq. (2). The results are shown in Fig. 4 for the ten considered reservoirs. Figure 4 displays also the corresponding time scales T_m and T_j, as well as the age distribution in a hypothetical, perfectly mixed reservoir of same volume as each of the ten considered reservoirs, i.e. Equation (5). In line with Eq. (4), all computed age distribution functions satisfy $\mu(0) = 1/T_m$. Figure S2 in Supplement presents the same results in the form of cumulated water age distributions, which confirm that the computed age distributions satisfy the identity displayed in Eq. (3).

The computed water age distribution functions shown in Fig. 4 are constant over a range of small values of water age, irrespective of the tested configuration, and in most cases,

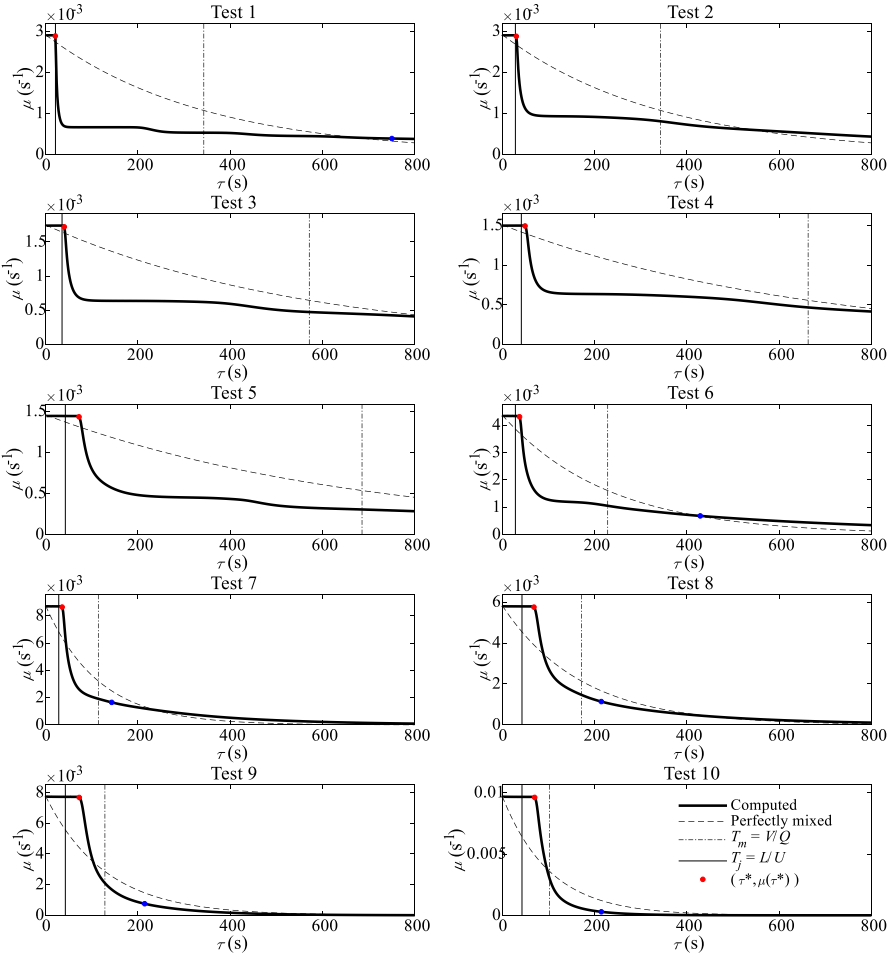

Fig. 4 Computed volume-averaged water age distribution, compared to the distribution corresponding to a perfectly mixed reservoir of same volume, as well as to the time scales T_m and T_j. The red marker (red dot) corresponds to the upper bound τ^* of the range where μ is uniform

they are characterized by a relatively long tail. This may be interpreted as the signature of a combination of fast and slow pathways that water particles travel along their routes through the reservoirs, as detailed hereafter.

3.1 Fast pathway

In all configurations, for relatively small values of τ, the age distribution μ remains uniform over a range extending from $\tau = 0$ up to a value noted τ^*, and displayed by a red marker in each plot of Fig. 4. Figure 5a compares τ^* to T_j. In all cases, τ^* and T_j are of the same order of magnitude, with τ^* varying between T_j (Test 1) and, at most, 1.7 times T_j.

In Fig. 5b, the ratio of τ^* to T_j is shown as a function of the reservoir aspect ratio L/B and its expansion ratio $\Delta B/b$. Three groups of configurations can be identified depending on the reservoir aspect ratio and expansion ratio.

3.1.1 Relatively short reservoirs

For relatively short reservoirs ($L/B < 1.5$), irrespective of the reservoir expansion, the value of τ^* does not exceed T_j by more than 20% (Tests 1–4). As shown in Figure S1 in Supplement, this corresponds to flow patterns involving a jet flowing straight from the reservoir inlet to its outlet, without reattachment on either of the sidewalls. To some extent, this flow type bears a resemblance to a plug flow over the jet region, which is consistent with a volume-averaged age distribution μ remaining close to uniform in the range $[0, \tau^*]$ with τ^* approximately equal to T_j.

In the case of the shortest reservoir (Test 1), the value of τ^* matches almost perfectly T_j (relative difference below 1%), reflecting the fast pathway similar to a plug flow used by water particles remaining in the straight jet. In Tests 2 to 4, the value of τ^* tends to increase with the reservoir aspect ratio L/B. This reflects a more pronounced deceleration of the jet in the case of relatively longer reservoirs, as can be observed in Figure S1b to d when compared to Figure S1a in Supplement.

The attribution of the plateau in the age distribution to the fast pathway constituted by the jet is further corroborated by looking at the cumulative age distribution function (CDF), as shown in Figure S2 in Supplement. For Test 1, Figure S2a indicates that the portion of

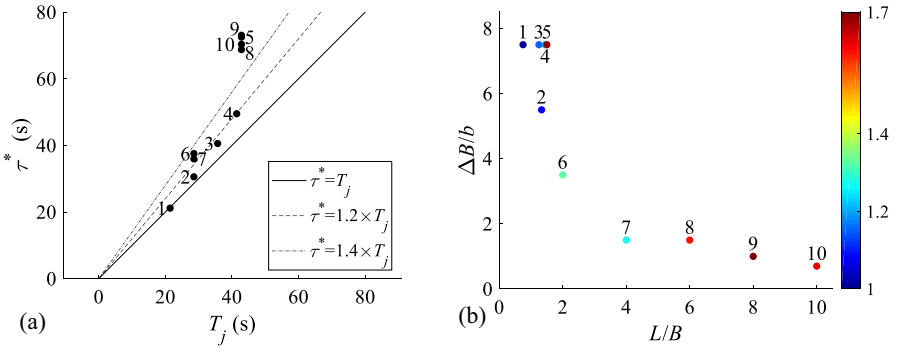

Fig. 5 **a** τ^* as a function of T_j, **b** ratio of τ^* to T_j (colour scale), as a function of the reservoir aspect ratio L/B and its expansion ratio $\Delta B/b$. The number next to each marker in the graphs indicates the corresponding test ID

water characterized by $\tau \leq \tau^*$ equals 6.1%. This agrees almost perfectly with the ratio of the volume occupied by an idealized jet without diffusion ($h\ b\ L$) to the entire reservoir volume ($h\ B\ L$), i.e. 6.3% (Table 3 and Figure S3 in Supplement). For Tests 2–4, a similar agreement is obtained, with deviations not exceeding one percentage point.

3.1.2 Reservoirs of intermediate length

When the reservoir length exceeds a certain threshold (here, $L/B \geq 1.5$), the flow pattern shifts from a straight, detached jet to a reattached jet. This shift leads to a substantial change in the value of the ratio of τ^* to T_j, as exemplified by the comparison between Test 4 and Test 5 (Fig. 5a). While both tests correspond to reservoirs of similar geometry (identical width, difference in length of 3%), the ratio of τ^* to T_j varies from 1.18 (Test 4) to 1.69 (Test 5). This rise by 40% in τ^*/T_j results from the curved shape of the reattached jet in Test 5, which increases the time spent in the jet by water particles travelling along this fast pathway.

In Tests 6 and 7, the flow patterns are comparable to that of Test 5. However, the ratio of τ^* to T_j is smaller ($\tau^*/T_j \sim 1.2$–1.3) than in the case of Test 5 ($\tau^*/T_j \sim 1.7$) because the expansion ratio is more limited in Tests 6 and 7 than in Test 5 (Table 2). Consequently, the extra time spent by water particles travelling along the curved, reattached jet is reduced in Tests 6 and 7 compared to the case of Test 5. This results from the *combined effect of a longer extra distance to be travelled in Test 5 and a more pronounced slow-down of the jet over this longer travel distance,* as revealed by the velocity fields in Figure S1 in Supplement.

In Tests 5 to 7, the portion of water characterized by $\tau \leq \tau^*$ exceeds greatly the ratio of the volume occupied by an idealized jet without diffusion to the entire reservoir volume, as shown in Table 3 and Figure S3 in Supplement.

3.1.3 Relatively long reservoirs

In the case of relatively long reservoirs ($L/B \geq 5$), the ratio of τ^* to T_j is found particularly high ($\tau^*/T_j > 1.6$). This may be explained by a twofold effect. While in reservoirs of intermediate length (Tests 5–7), high values of τ^*/T_j result mostly from a comparatively longer distance travelled by the jet compared to a straight jet, in the case of relatively long reservoirs (Tests 8–10) not only the distance travelled by the jet is longer but also, due to the presence of a second reattachment, the jet almost vanishes at a certain distance of the inlet and the flow becomes spread over the whole width of the reservoir (Figure S1h to j in Supplement). This leads to a drop in the velocity, which explains the relatively high values of τ^* obtained compared to T_j. For relatively long reservoirs, the portion of water characterized by $\tau \leq \tau^*$ exceeds by about 60% the ratio of the volume occupied by an idealized jet to the

Table 3 Portion CDF(τ^*) of the reservoir volume corresponding to fast pathway, and ratio of the volume of an idealized jet without diffusion ($h\ b\ L$) to the entire reservoir volume ($h\ B\ L$)

Test ID	1 (%)	2 (%)	3 (%)	4 (%)	5 (%)	6 (%)	7 (%)	8 (%)	9 (%)	10 (%)
CDF(t^*)	6.1	8.8	7.0	7.3	10	16	31	40	56	68
b/B	6.3	8.3	6.3	6.3	6.3	13	25	25	33	42%

entire reservoir volume (Table 3 and Figure S3 in Supplement), due to the jet elongation, slow-down and spread over the entire width in the downstream portion of the reservoir.

3.2 Slow pathways

3.2.1 Sequence of steps

Figure 6 shows the same results as in Fig. 4, but a logarithmic scale is used in the vertical axis, and water age in the horizontal axis is scaled by the characteristic time T_j. In the case of Test 1, Fig. 6 reveals that for values of τ exceeding τ^*, $\mu(\tau)$ remains also uniform for τ/T_j in the range of about 2–9, as well as in the range of about 12–19.

Hence, for values of τ situated between zero and approximately 19 times T_j, the age distribution function $\mu(\tau)$ can be considered as decreasing by steps, with smooth transitions

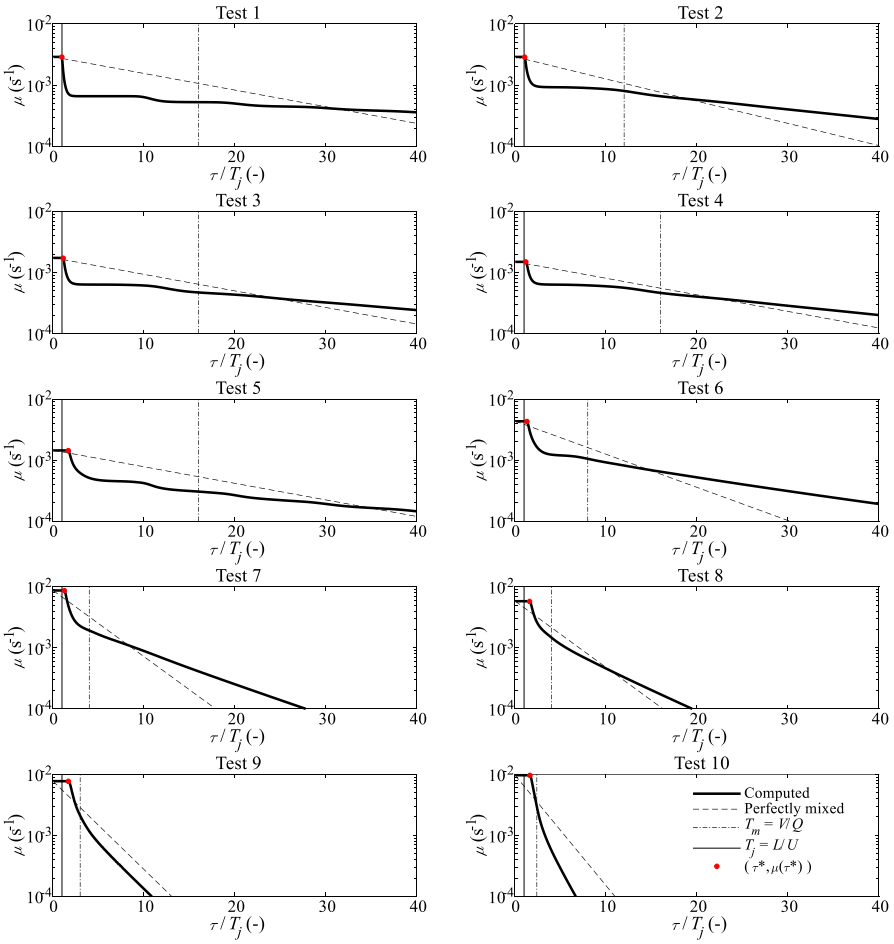

Fig. 6 Same as Fig. 4, but a logarithmic scale is used for the vertical axis and, in the horizontal axis, the age τ has been scaled by the characteristic time T_j

between the successive steps. This may be interpreted as the signature of the diffusion of water particles between the main jet and the two lateral recirculations (Figure S1), leading to some particles travelling solely in the main jet, while others recirculate a number of times in the vortices before reaching the reservoir outlet. The "delay" affecting the water particles temporarily captured in the recirculations is reflected by the length of the successive steps, which relates to the time needed for water particles to complete a passage in a large recirculation [48, 54]. When τ exceeds about 20 times T_j, the steps are no more perceptible in the graphs of $\mu(\tau)$, which appears to decline smoothly.

For Tests 2–6, a similar step as in the case of Test 1 can be observed for τ over T_j varying between approximately 2 and 9. In contrast, in the case of Tests 7–8 (flow patterns with two reattachment points), such steps in the age distribution function are hardly perceptible.

3.2.2 Exponential decay

For even larger values of τ, the age distribution function $\mu(\tau)$ tends to decay exponentially, as demonstrated by the straight lines visible for large values of τ in the representation of $\mu(\tau)$ in Fig. 6. This is even more obvious in Figure S4 in Supplement, which displays the same information as in Fig. 6 but with a horizontal axis extending over a broader range of values. Only in the case of Test 5, it is not entirely clear whether the distribution tends towards a straight line (Fig. 6 and Figure S4) and, hence, whether $\mu(\tau)$ declines exponentially for large values of τ.

The slope of the straight lines visible in Fig. 6 and Figure S4 differs from the slope of the line representing the theoretical age distribution in a perfectly mixed reservoir. In most cases, the slope of the computed water age distribution μ is milder than the theoretical one, which suggests that the portion of the reservoir which operates similarly to a perfectly mixed reservoir is characterized by a larger time scale than T_m. This results probably from a the relatively low flow rate involved. Nonetheless, for Test 9, the slope of the straight part representing the computed age distribution function in Fig. 5 and Figure S4 seems very close to that of the theoretical distribution for a perfectly mixed reservoir, and the former becomes even steeper than the latter in the case of Test 10.

Based on visual inspection of Figure S4, we estimated an approximate value of water age above which each reservoir operates similarly to a perfectly mixed reservoir. This value of τ is represented by a blue marker in Figure S4 as well in Figure S2. Using Figure S2, it can be inferred that in most cases the fraction of the reservoir volume which operates similarly to a perfectly mixed reservoir ranges between 30 and 55%, except in the case of Tests 9 and 10 for which this fraction is below 10%. This relates to the jet spreading over the whole reservoir width in the downstream part of the reservoirs considered in Tests 9 and 10.

These results are consistent with findings by Mouchet et al. (2012) [55] for the ocean. They also observed an exponential decay for large values of τ, suggesting that for relatively old water particles, the ocean operates similarly to a perfectly mixed reservoir. In other words, *above some age, the probability to escape the main flow and, subsequently, leave the reservoir is the same for all particles, whatever their age* [55].

3.2.3 Length of the tails

In Figure S2, green markers show the 90th percentile of the age distribution. It is used here as an indicator of the length of the tail of the distributions. The corresponding values are

also reported in Table 4. For the relatively long reservoirs (Tests 8 to 10), the 90th percentile of water age corresponds to 1–3 times the characteristic time T_m. In the other cases, the ratio of the 90th percentile of water age to T_m is substantially higher, with values between 4 and 9.

4 Discussion

4.1 Simple model

The volume-averaged water age distributions displayed in Fig. 4 exhibit patterns which we attribute to a combination of a fast pathway (main jet) and several slower pathways (recirculations). As such, the water age distributions act as a signature of the flow fields which develop in the considered reservoirs. Below, we outline a conceptual model, aimed at further exploring this interpretation. The model was designed to be as simple as possible, while still reproducing some key features of the water age distributions of interest. For the sake of simplicity, the model is only developed for the cases involving flow fields with a straight, detached jet (Tests 1–4), while the geometric peculiarities of curved, reattached jets are not incorporated in the model. The conceptual model is not intended to be used for making predictions for real-world cases, since it is not able to grasp the complexity of turbulent flow processes observed in real reservoirs, but it points at the main mechanisms explaining the computed age distribution functions.

4.1.1 Model concept

In the proposed model, the reservoir is assumed to contain a mix of water particles, each of them following either the fast pathway (main jet) or slow pathways (recirculations). The particles following the slow pathways have accumulated various delays compared to the water particles travelling along the fast pathway. The delay is linked to a typical time $\Delta \tau$ taken by water particles to recirculate once in the vortices located on either side of the main jet (Figure S1a to d). Not all water particles following slow pathways encounter the same delay since they have not all recirculated the same number of times in the vortices.

4.1.2 Mathematical formulation

In the model, we consider N classes of water particles, each corresponding to particles having recirculated a specific number of times in the vortices. The pathways of particles travelling along slow pathways are idealized as "elongated" jets, i.e. jets in which the travel time is simply incremented by a multiple of $\Delta \tau$ compared to the travel time T_j in the main jet.

Table 4 Ratio of water age τ_{90} to T_m, with τ_{90} corresponding to the 90th percentile of the volume-averaged water age distribution μ

Test ID	1	2	3	4	5	6	7	8	9	10
τ_{90}/T_m	9.1	5.2	4.9	4.0	9.8	5.5	4.0	2.8	1.6	1.1

Therefore, the age distribution for a particular class n of particles is given by an expression similar to Eq. (7):

$$\frac{1}{T_j + n\ \Delta\tau} H\left(T_j + n\ \Delta\tau - \tau\right) \text{ with } n = 0 \ldots N, \tag{8}$$

As suggested by Fig. 6a, the unitary delay $\Delta\ \tau$ may be linked to the time scale T_j, as follows: $\Delta\ \tau = \alpha\ T_j$, with α a model coefficient to be determined. In the case of Test 1, Fig. 6a hints that α takes a value of the order of 10. By setting n set to zero in Eq. (8), this equation also describes the age distribution function of particles following the fast pathway.

We assume that all classes of water particles are not populated similarly. The relative population of each class is linked to the probability θ of a water particle to be captured in a vortex (for $n = 1$) or captured again just after having recirculated in this vortex (for $n > 1$). Therefore, the relative population φ_n of class n may be evaluated as:

$$\varphi_n = \varphi_0 \theta^n \tag{9}$$

with φ_0 the relative population in class $n = 0$ (i.e., particles travelling along the fast pathway), which needs to be determined. Consequently, the volume-averaged water age distribution in the reservoir is given by:

$$\mu(\tau) = \sum_{n=0}^{N} \left[\varphi_0\ \theta^n \frac{1}{T_j + n\ \Delta\tau} H\left(T_j + n\ \Delta\tau - \tau\right) \right] \tag{10}$$

4.1.3 Parameters identification

Properties (3) and (4) of the volume-averaged water age distributions may be used to constrain the values of the model parameters θ and φ_0. Plugging Eq. (10) into Eq. (3) leads to:

$$\int_0^{\infty} \mu(\tau)\, d\tau = \varphi_0 \sum_{n=0}^{N} \theta^n = \varphi_0 \frac{1 - \theta^n}{1 - \theta} = 1 \tag{11}$$

For $N \to \infty$, it comes: $\theta = 1 - \varphi_0$. Hence, θ and φ_0 may not be chosen arbitrarily. Their values must be set consistently so that identity (3) is satisfied by the model prediction. Similarly, satisfying Eq. (4) requires that:

$$\mu(0) = \varphi_0 \sum_{n=0}^{N} \left(\frac{\theta^n}{T_j + n\ \Delta\tau} \right) = \frac{1}{T_m} \tag{12}$$

Equations (11) and (12) are two nonlinear equations for θ and φ_0 which enable setting the values of these two parameters without calibration.

4.1.4 Model application

The model was applied to Test 1 by considering $N = 1000$. It leads to the results shown in Fig. 7, which are found independent of N provided that N exceeds about 100. In light of the parsimony of the model, it may be considered that the upper panel of Fig. 7 compares fairly well with Fig. 4a and the lower one with Figure S4a (also the exponential decay appears

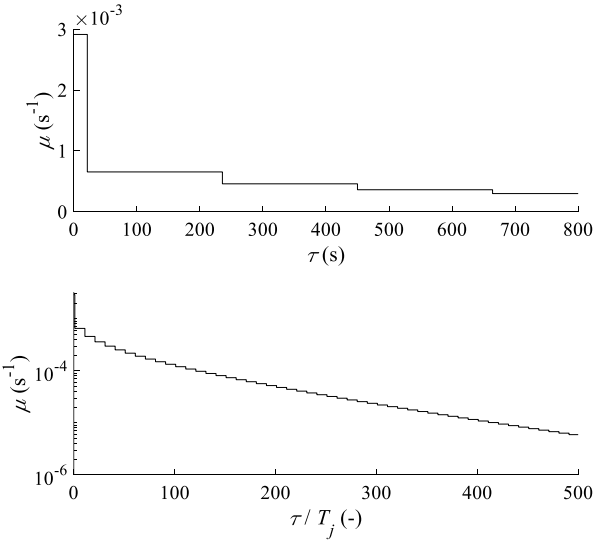

Fig. 7 Age distribution function μ calculated for Test 1 based on the conceptual model with Δ $\tau = 10\ T_j$ and $N = 1000$

too "slow" in the model result), suggesting that the conceptual model captures key features of the processes studied here, and supporting the interpretation of the patterns in the water age distributions.

4.2 Possible role of stratification

Throughout this study, stratification was neglected in our 2D depth-averaged modelling framework, and the water column was assumed to be vertically well mixed. In real-world shallow stormwater ponds, stratification was observed to be important in some circumstances [56, 57]. Depth-averaged modelling might hence be viewed as a limitation. Nonetheless, in the studied configurations, stratification remains limited. There are mainly two reasons for this.

First, the inlet and outlet of the reservoirs considered here are free surface channels. Consequently, the inlet jet is distributed over the whole flow depth and is not concentrated on just a fraction of the flow depth. This differs from real-world stormwater ponds in which pressurized pipes are used as inlets and outlets (with their inverts typically close to pond bed) leading to a concentrated inlet jet near the bottom [56]. Second, thermal, chemical and densimetric stratifications are reported in the field, with variations in fluid density, temperature, and salt concentration over relatively long periods of time (days, seasons, years) [56, 57]. This contrasts with the experimental reservoirs studied here, which were fed with water only, at a constant temperature, and for durations not exceeding about an hour.

Some authors included stratification dynamics in their time scales; but they focused on deep water bodies, such as natural stratified lakes [58], which considerably differ from the shallow man-made reservoirs considered here, which are less prone to stratification.

From the perspective of the reservoir hydrodynamics, the 2D flow computations on which we build here were extensively verified against laboratory experiments. An Ultrasonic Doppler Velocity Profiler (Metflow SA, UVP-DUO) was utilized to measure velocity profiles over the flow depth [35]. The observations confirmed that the velocity profiles were mainly uniform over the flow depth, and the vertical velocity component remained

small compared to the horizontal one, reflecting the 2D-horizontal character of the flow [35]. In a similar setting, "reasonable" two-dimensionality of the flow was verified based on dye visualization [24]. Moreover, the measured flow patterns could be repeatedly reproduced by several 2D depth-averaged flow models as used here [26, 37, 39, 52].

5 Conclusion

The distribution function of the volume-averaged water age in rectangular shallow reservoirs was calculated for ten different experimental reservoir layouts. These distribution functions contain the signature of all key features of the fast and slow pathways travelled by water particles along their routes across the reservoirs. As such, the distribution function of the volume-averaged water age provides valuable information for assessing the hydraulic performance of shallow reservoirs, and proves helpful for the practical design and sizing of shallow reservoirs.

Three main regions may be distinguished in all computed distribution functions. First, irrespective of the reservoir layout, the distribution functions were found uniform over a range of small values of water age. This corresponds to particles travelling along the main jet, without being captured in recirculation zones. Second, the functions show a sequence of decreasing steps for larger values of water age. Each of these steps corresponds to a range in which the distribution function remains also uniform. This corresponds to water particles being captured by one of the large recirculations and recirculating a number of times in the vortices before leaving the reservoir. These water particles reach the reservoir outlet with a "delay" reflected by the length of the successive steps in the distribution functions. Third, for large values of water age, the age distribution functions tend to an exponential decay, in line with the standard observation that for "old" water particles the reservoir operates similarly to a well-mixed reservoir.

The computed distribution functions reflect a combination of fast (main jet) and slower (multiple passages in the large recirculations) pathways. This interpretation was embedded in a parsimonious conceptual model, whose only purpose is to help understanding the link between the shape of the age distribution functions and the underpinning flow processes. Model parameters were set based on physical constraints, without any calibration. The model was shown to qualitatively reproduce the key features of the distribution function, namely the sequence of steps and a decay close to an exponential one.

The present study contains several limitations. While the reservoir geometry was systematically varied, future studies should also consider variations in the hydraulic boundary conditions, as well as effects of unsteadiness. The methodological framework developed here should be extended to a 3D description of flow and tracer transport to account for possible stratification, as well as to more complex reservoir layouts (e.g., non-rectangular, involving baffles, islands or berms). Future work should also include the study of sediment age besides water age.

Supplementary Information The online version contains supplementary material available at https://doi.org/10.1007/s10652-024-09967-z.

Author contributions ED, BD and PA conceptualized the research and designed the methodology. BD and PA developed the computer codes for data analysis and performed formal analysis. BD wrote the original draft, which was revised by SE and ED MP provided expertise.

Funding No funding was received for conducting this study.

Declarations

Conflict of interest The authors declare no competing interests.

References

1. Dufresne M, Vazquez J, Terfous A, Ghenaim A, Poulet J-B (2009) Experimental investigation and CFD modelling of flow, sedimentation, and solids separation in a combined sewer detention tank. Comput Fluids 38:1042–1049
2. Isenmann G, Dufresne M, Vazquez J, Mose R (2017) Bed turbulent kinetic energy boundary conditions for trapping efficiency and spatial distribution of sediments in basins. Water Sci Technol 76:2032–2043
3. Sebastian C, Becouze-Lareure C, Lipeme Kouyi G, Barraud S (2014) Event-based quantification of emerging pollutant removal for an open stormwater retention basin - loads, efficiency and importance of uncertainties. Water Res 72:239–250
4. Tsavdaris A, Mitchell S, Williams JB (2015) Computational fluid dynamics modelling of different detention pond configurations in the interest of sustainable flow regimes and gravity sedimentation potential. Water Environ J 29:129–139
5. Adamsson Å, Stovin V, Bergdahl L (2003) Bed shear stress boundary condition for storage tank sedimentation. J Environ Eng 129:651–658
6. Guzman CB, Cohen S, Xavier M, Swingle T, Qiu W, Nepf H (2018) Island topographies to reduce short-circuiting in stormwater detention ponds and treatment wetlands. Ecol Eng 117:182–193
7. Persson J, Wittgren HB (2003) How hydrological and hydraulic conditions affect performance of ponds. Ecol Eng 21:259–269
8. Persson J (2000) The hydraulic performance of ponds of various layouts. Urban Water 2:243–250
9. Persson J, Somes NLG, Wong THF (1999) Hydraulics efficiency of constructed wetlands and ponds. Water Sci Technol 40:291–300
10. Liu X, Xue H, Hua Z, Yao Q, Hu J (2013) Inverse calculation model for optimal design of rectangular sedimentation tanks. J Environ Eng (US) 139:455–459
11. Lakzian E, Saghi H, Kooshki O (2020) Numerical simulation of sediment deposition and trapping efficiency estimation in settling basins, considering secondary flows. Int J Sedim Res 35:347–354
12. Izdori F, Semiao AJC, Perona P (2019) The role of environmental variables in waste stabilization ponds' morphodynamics. Front Environ Scince 7:159
13. Goula AM, Kostoglou M, Karapantsios TD, Zouboulis AI (2008) A CFD methodology for the design of sedimentation tanks in potable water treatment. Case study: the influence of a feed flow control baffle. Chem Eng J 140:110–121
14. Zhang J-M, Lee HP, Khoo BC, Peng KQ, Zhong L, Kang C-W, Ba T (2014) Shape effect on mixing and age distributions in service reservoirs. J Am Water Works Assoc 106:E481–E491
15. Claude N, Secher M, Deng J, Valette E, Duclercq M (2020) Numerical modeling of flow and sediment transport in a real shallow reservoir: Comparison between 2D and 3D simulation. In: *River Flow 2020-Proceedings of the 10th Conference on Fluvial Hydraulics*, (pp. 331–339)
16. Dufresne M, Vazquez J, Terfous A, Ghenaim A, Poulet J-B (2009) CFD modeling of solid separation in three combined sewer overflow chambers. J Environ Eng 135:776–787
17. Tarpagkou R, Pantokratoras A (2013) CFD methodology for sedimentation tanks: the effect of secondary phase on fluid phase using DPM coupled calculations. Appl Math Model 37:3478–3494
18. Li H, Sansalone J (2021) CFD with evolutionary optimization for stormwater basin retrofits. J Environ Eng (US) 147:04021017
19. Rowland JC, Stacey MT, Dietrich WE (2009) Turbulent characteristics of a shallow wall-bounded plane jet: Experimental implications for river mouth hydrodynamics. J Fluid Mech 627:423–449
20. Canestrelli A, Nardin W, Edmonds D, Fagherazzi S, Slingerland R (2014) Importance of frictional effects and jet instability on the morphodynamics of river mouth bars and levees. J Geophys Res Oceans 119:509–522

21. Milovanovic I, Bareš V, Hedström A, Herrmann I, Picek T, Marsalek J, Viklander M (2020) Enhancing stormwater sediment settling at detention pond inlets by a bottom grid structure (BGS). Water Sci Technol 81:274–282
22. Grayman WM, Rossman LA, Deininger RA, Smith CD, Arnold CN, Smith JF (2004) Mixing and aging of water in distribution system storage facilities. J Am Water Works Assoc 96:70–80
23. Stovin VR, Saul AJ (2000) Computational fluid dynamics and the design of sewage storage chambers. Water Environ J 14:103–110
24. Dufresne M, Dewals BJ, Erpicum S, Archambeau P, Pirotton M (2010) Classification of flow patterns in rectangular shallow reservoirs. J Hydraul Res 48:197–204
25. Peltier Y, Erpicum S, Archambeau P, Pirotton M, Dewals B (2014) Experimental investigation of meandering jets in shallow reservoirs. Environ Fluid Mech 14:699–710
26. Dewals BJ, Kantoush SA, Erpicum S, Pirotton M, Schleiss AJ (2008) Experimental and numerical analysis of flow instabilities in rectangular shallow basins. Environ Fluid Mech 8:31–54
27. Choufi L, Kettab A, Schleiss AJ (2014) Bed roughness effect on flow field in rectangular shallow reservoir [Effet de la rugosité du fond d'un réservoir rectangulaire à faible profondeur sur le champ d'écoulement], *Houille Blanche* 83–92.
28. Camnasio E, Orsi E, Schleiss AJ (2011) Experimental study of velocity fields in rectangular shallow reservoirs. J Hydraul Res 49:352–358
29. Goltsman, A., and Saushin, I. (2019) Flow pattern of double-cavity flow at high Reynolds number, *Physics of Fluids 31*.
30. Miozzi M, Romano GP (2020) Propagation of perturbations and meandering in a free surface shallow water jet. Experiments Fluids 61:065101
31. Camnasio E, Erpicum S, Orsi E, Pirotton M, Schleiss AJ, Dewals B (2013) Coupling between flow and sediment deposition in rectangular shallow reservoirs. J Hydraul Res 51:535–547
32. Dufresne M, Dewals BJ, Erpicum S, Archambeau P, Pirotton M (2010) Experimental investigation of flow pattern and sediment deposition in rectangular shallow reservoirs. Int J Sedim Res 25:258–270
33. Yan H, Vosswinkel N, Ebbert S, Lipeme Kouyi G, Mohn R, Uhl M, Bertrand-Krajewski J-L (2020) Numerical investigation of particles' transport, deposition and resuspension under unsteady conditions in constructed stormwater ponds. Environ Sci Europe 32:1–17
34. Dominic JA, Aris AZ, Sulaiman WNA, Tahir WZWM (2016) Discriminant analysis for the prediction of sand mass distribution in an urban stormwater holding pond using simulated depth average flow velocity data. Environ Monit Assess 188:1–15
35. Kantoush SA, De Cesare G, Boillat JL, Schleiss AJ (2008) Flow field investigation in a rectangular shallow reservoir using UVP LSPIV and numerical modelling. Flow Meas Instrum 19:139–144
36. Peltier Y, Erpicum S, Archambeau P, Pirotton M, Dewals B (2015) Can meandering flows in shallow rectangular reservoirs be modeled with the 2D shallow water equations? J Hydraul Eng 141:04015008
37. Dufresne M, Dewals BJ, Erpicum S, Archambeau P, Pirotton M (2011) Numerical investigation of flow patterns in rectangular shallow reservoirs. Eng Appl Comput Fluid Mech 5:247–258
38. Ferrara V, Erpicum S, Archambeau P, Pirotton M, Dewals B (2018) Flow field in shallow reservoir with varying inlet and outlet position. J Hydraul Res 56:689–696
39. Kantoush SA, Bollaert E, Schleiss AJ (2008) Experimental and numerical modelling of sedimentation in a rectangular shallow basin. Int J Sedim Res 23:212–232
40. Esmaeili T, Sumi T, Kantoush SA, Haun S, Rüther N (2016) Three-dimensional numerical modelling of flow field in shallow reservoirs. Proc Inst Civ Eng Water Manag 169:229–244
41. Zahabi H, Torabi M, Alamatian E, Bahiraei M, Goodarzi M (2018) Effects of geometry and hydraulic characteristics of shallow reservoirs on sediment entrapment. Water (Switzerland) 10:1725
42. Lucas LV, Deleersnijder E (2021) Tracers and timescales: Tools for distilling and simplifying complex fluid mechanical problems. Water (Switzerland) 13:2796
43. Deleersnijder E, Delhez EJM (2007) Timescale- and tracer-based methods for understanding the results of complex marine models. Estuar Coast Shelf Sci 74:v–vii
44. Deleersnijder E, Campin J-M, Delhez EJM (2001) The concept of age in marine modelling I. Theory and preliminary model results. J Mar Syst 28:229–267
45. Bolin B, Rodhe H (1973) A note on the concepts of age distribution and transit time in natural reservoirs. Tellus 25:58–62
46. Monsen NE, Cloern JE, Lucas LV, Monismith SG (2002) A comment on the use of flushing time, residence time, and age as transport time scales. Limnol Oceanogr 47:1545–1553
47. Takeoka H (1984) Fundamental concepts of exchange and transport time scales in a coastal sea. Cont Shelf Res 3:311–326

48. Xavier MLM, Janzen JG (2017) Effects of inlet momentum and orientation on the hydraulic performance of water storage tanks. Appl Water Sci 7:2545–2557
49. Moncho-Esteve IJ, Palau-Salvador G, Brevis W, Vaas MO, López-Jiménez PA (2015) Numerical simulation of the hydrodynamics and turbulent mixing process in adrinking water storage tank. J Hydraul Res 53:207–217
50. Sonnenwald F, Guymer I, Stovin V (2018) Computational fluid dynamics modelling of residence times in vegetated stormwater ponds. Proc Inst Civ Eng Water Manag 171:76–86
51. Dewals B, Archambeau P, Bruwier M, Erpicum S, Pirotton M, Adam T, Delhez E, Deleersnijder E (2020) Age of water particles as a diagnosis of steady-state flows in shallow rectangular reservoirs. Water (Switzerland) 12:2819
52. Camnasio E, Erpicum S, Archambeau P, Pirotton M, Dewals B (2014) Prediction of mean and turbulent kinetic energy in rectangular shallow reservoirs. Eng Appl Comput Fluid Mech 8:586–597
53. Erpicum S, Meile T, Dewals BJ, Pirotton M, Schleiss AJ (2009) 2D numerical flow modeling in a macro-rough channel. Int J Numer Meth Fluids 61:1227–1246
54. Stamou AI (2002) Verification and application of a mathematical model for the assessment of the effect of guiding walls on the hydraulic efficiency of chlorination tanks. J Hydroinf 4:245–254
55. Mouchet A, Deleersnijder E, Primeau F (2012) The leaky funnel model revisited. Tellus Ser A Dyn Meteorol Oceanograph 64:19131
56. Ahmed SS, Loewen MR, Zhang W, Ghobrial TR, Zhu DZ, Mahmood K, van Duin B (2022) Field observations of stratification in stormwater wet ponds. J Environ Manag 322:115988
57. Song K, Xenopoulos MA, Buttle JM, Marsalek J, Wagner ND, Pick FR, Frost PC (2013) Thermal stratification patterns in urban ponds and their relationships with vertical nutrient gradients. J Environ Manag 127:317–323
58. Pilotti M, Simoncelli S, Valerio G (2014) A simple approach to the evaluation of the actual water renewal time of natural stratified lakes. Water Resour Res 50:2830–2849